Structural Engineering and Mechanics, Vol. 20, No. 6 (2005) 695-712 695
DOI: http://dx.doi.org/10.12989/sem.2005.20.6.695

Experimental studies on seismic behavior of steel coupling beams

Wan-Shin Park† and Hyun-Do Yun‡

School of Architecture, Chungnam National University, Daejeon 305-764, Korea

Jae-Yong Chung‡†

Department of Architecture, Hongik University, Seoul 121-791, Korea

Yong-Chul Kim‡‡

School of Architecture, Chungnam National University, Daejeon 305-764, Korea

(Received November 10, 2004, Accepted April 11, 2005)

Abstract. Hybrid coupled shear walls in tall buildings are known as efficient structural systems to provide lateral resistance to wind and seismic loads. Multiple hybrid coupled shear walls throughout a tall building should be joined to provide additional coupling action to resist overturning moments caused by the lateral loading. This can be done using a coupling beam which connects two shear walls. In this study, experimental studies on the hybrid coupled shear wall were carried out. The main test variables were the ratios of coupling beam strength to connection strength. Finally, this paper provides background for rational design guidelines that include a design model to behave efficiently hybrid coupled shear walls.

Key words: steel coupling beams; connection failure; shear yielding; flexure yielding; hybrid coupled shear walls.

1. Introduction

In the last decade, coupled flexural walls have, increasingly, become recognised as efficient lateral load resisting systems for tall buildings. Coupled shear walls exhibit considerable lateral stiffness and strength as well as providing an architecturally practical structural system. Coupled shear walls consist of two or more in-plane shear walls inter-connected with coupling beams. The presence of moment resistant connections between the beams and the shear walls serve to stiffen the shear wall system laterally. Under lateral loads, each shear wall behave as a cantilever as well as resisting the external moment with a coupled formed by opposing axial loads in the walls. Structural steel

† Part-Time Lecturer, Ph.D.
‡ Associate Professor, Ph.D., Corresponding author, E-mail: wiseroad@cnu.ac.kr
‡† Assistant Professor, Ph.D.
‡‡ Graduate Student

coupling beams provide a viable alternative to reinforced concrete coupling beams, particularly where height restrictions do not permit the use of deep reinforced concrete or composite coupling beams, or where the required capacity and stiffness cannot be developed economically by a conventionally reinforced concrete coupling beam.

Previous researchers (Park and Yun 2005, Park *et al.* 2005, El-Tawil and Kuenzli 2002) have shown that the lateral stiffness and strength of concrete shear walls can be significantly increased by coupling the shear walls using embedded steel beams. This new concept in coupled wall design is currently being pursued by Shahrooz *et al.* (1993, 2002, 2004a, 2004b) at the University of Cincinnati and by Harries (1995, 2001) at McGill University. Shahrooz *et al.* (1993) tested three specimens consisting of the stub of a coupling beam projecting from a segment of wall. The coupling beam was loaded vertically in a reversed cyclic manner. The tests investigated the effects of axial load in the wall and of reinforcing bars being welded to the embedded member.

The calculation of the embedment capacity was based on the model presented by Mattock and Gaafar (1982). The preliminary research conducted by Harries (2001) for this program involved the testing of two full-scale segments of a coupled wall (two walls coupled by a beam). No current design methods are especially available for computing the required embedment length of steel coupling beams, taking into account the contribution of the auxiliary bars and the horizontal ties on the top and bottom flanges of an embedded steel section. The model proposed in this study for computing the required embedment length of steel coupling beams is evaluated for its reliability.

The objective of this research was to investigate seismic behavior of steel coupling beams in terms of the failure mechanism, hysteretic response, strength, dissipated energy characteristics, stresses and the strains by conducting experimental studies. The main test variables were the ratios of coupling beam strength to connection strength. Finally, this paper provides background for rational design guidelines that include a design model to behave efficiently hybrid coupled shear walls.

2. Prototype structure

The test specimens represented a subassembly at the 37th floor of an imaginary prototype structure, a 50-storey, three-bay by eight-bay office assumed to be located in International Building Code seismic zone 4 (IBC 2000). The structure is comprised of five reinforced concrete walls linked to form the central core, flat slab system, and perimeter steel frames. The typical floor plan is shown in Fig. 1.

2.1 Design of reinforced concrete shear wall

The prototype structure was designed for the combined effects of gravity and earthquake load according to the IBC provisions for concrete structures (IBC 2000). The reinforced concrete shear walls were proportioned and detailed following the IBC provisions (IBC 2000) and seismic provisions of ACI 318-05 (2005). The thickness of the shear walls in the region of the embedment will be partially governed by the width of the embedded steel coupling beam flange, which must fit within the vertical wall steel. For applications with larger coupling beams, channel shaped walls would become an appropriate design solution.

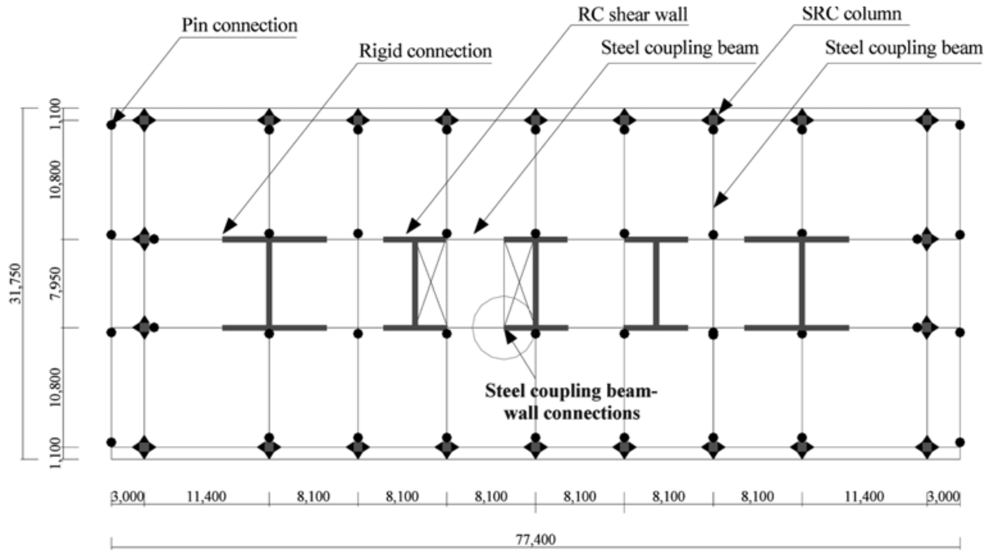

Fig. 1 Typical plan of prototype structure (dimension: mm)

2.2 Design of steel coupling beams

The design moment and shear in the 37th floor coupling beam are the largest of those of any floor. Hence, the coupling beams were more important at this location. The coupling beams are assumed to be structural steel members embedded in concrete door lintels over doors into the boundary element and interfacing them with the boundary element vertical bars and hoops. The steel coupling beams were designed in accordance with the seismic design requirements for link beams in eccentrically braced frames of the AISC steel design standard (2002).

For shear critical steel coupling beams, V_u is taken as 1.5 times the plastic shear capacity of the steel member, V_p

$$V_u = 1.5V_p = 1.5 \times 0.6F_y(h - 2t_f)t_w \tag{1}$$

For flexure critical steel beams, the shear capacity may be taken as the shear corresponding to the development of the plastic moment capacity:

$$V_f = 1.35\frac{2M_n}{L\phi_s} = 1.5\frac{2M_n}{L} \tag{2}$$

2.3 Design of embedment length

Due to lack of information, current design methods to calculate embedment length are tacit about cases in which hybrid coupled walls have connection details of stud bolts and horizontal ties on the top and bottom flanges of an embedded steel section. Based on the observation of the test results from a previous study (Gong *et al.* 2000), stud bolts and horizontal ties on the top and bottom flange of an embedded steel coupling beam section were specified in an effort to improve the

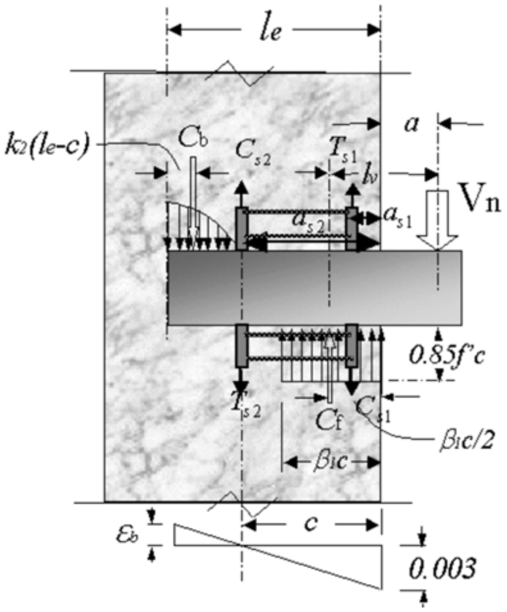

Fig. 2 Proposed models for calculating embedment length

stiffness and to improve the transfer of the flange-bearing force to the surrounding concrete. The contribution of the stud bolts and the horizontal ties are not considered in the existing models. Model E was used to calculate embedment lengths, taking into account the contribution of the auxiliary bars and the horizontal ties, as shown in Fig. 2. Park *et al.* (2005) proposed the following equation for strength of steel coupling beam-wall connections by taking moments about the centre of action of C_b to calculate embedment lengths

$$V_{r(proposed)} = f_b \beta_1 b l_e \left(\frac{0.58 - 0.22\beta_1}{0.88 + a/l_e}\right) + \frac{2(0.88 - a/l_e)\sum_{i=1}^{n} A_{si} f_{si}}{0.88 + a/l_e} \text{ (N)} \tag{3a}$$

where

$$f_b = 4.5\sqrt{f_c'}\left(\frac{t}{b}\right)^{0.60} \text{ (MPa)} \tag{3b}$$

where β_1 = ratio of the depth equivalent rectangular stress distribution to the depth of flexural compression zone as specified in Section 10.2.7 of ACI 318-05, A_{si} is the cross-sectional area of the auxiliary bar, i, inside the connections, f_{si} is the stress of the auxiliary bar, i, inside the connections, and T_{si} is the tensile force of the auxiliary bar, i, inside the connections.

Fig. 3 shows a comparison of the measured and predicted value from the equations proposed in this study. The previous researches (Park *et al.* 2005) are used to verify the proposed equation for bearing strength of steel coupling beam-wall connections. Based on the test results, the predicted values from equation proposed in this study for specimens HCWS-ST, HCWS-SB, and HCWS-SBVRT ranged from 1.00 to 1.11 of measured strengths, with standard deviations of 0.12 to 0.17. As shown in Fig. 3, the predicted values from the proposed equations are in good agreement with

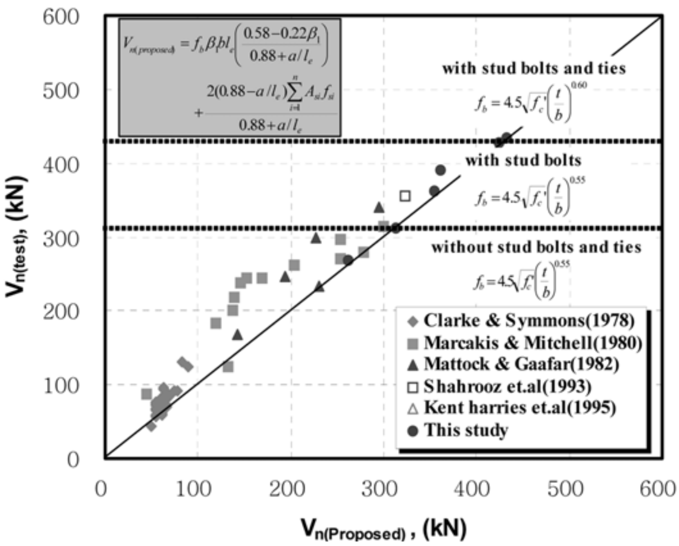

Fig. 3 Comparison of predicted values by proposed equation and observed strength

the measured strengths. The embedment lengths were calculated based on the Eq. (3a) proposed by authors, considering the contribution of the auxiliary bars and the horizontal ties.

3. Experimental program

3.1 Test specimens

The overall wall and beam dimensions of specimens are summarized in Fig. 4. The test subassemblies consisted of one half of the length of the coupling beam at the 37th floor. The test variables and details used in this study are summarized in Tables 1 and 2.

3.2 Material properties

The specimens were cast vertically, but typical construction joints in the wall around the connections were not reproduced. Ready-mix concrete with a minimum specified 28-day compressive strength of 30.0 MPa was used for each of the three specimens. The maximum size of the concrete aggregate was 15 mm to ensure good compaction of the concrete in the test specimens. The slump of the concrete was 150 mm. For each batch, the cylinders were constructed to measure the compressive strength of the concrete. The measured concrete strength and the elastic modulus were tested using the method defined in the ASTM standards. The horizontal and vertical reinforcement consisted of 13 mm diameter deformed bars. The reinforcing steel used for all the walls was obtained from a single batch of steel for each bar diameter, and three specimens were tested from each diameter of reinforcing used. Tension tests were conducted on full-sized bar samples in accordance with ASTM Standard A370 to determine the yield strength, ultimate strength, and total elongation. The observed material properties are reported in Tables 3 and 4, and Fig. 5.

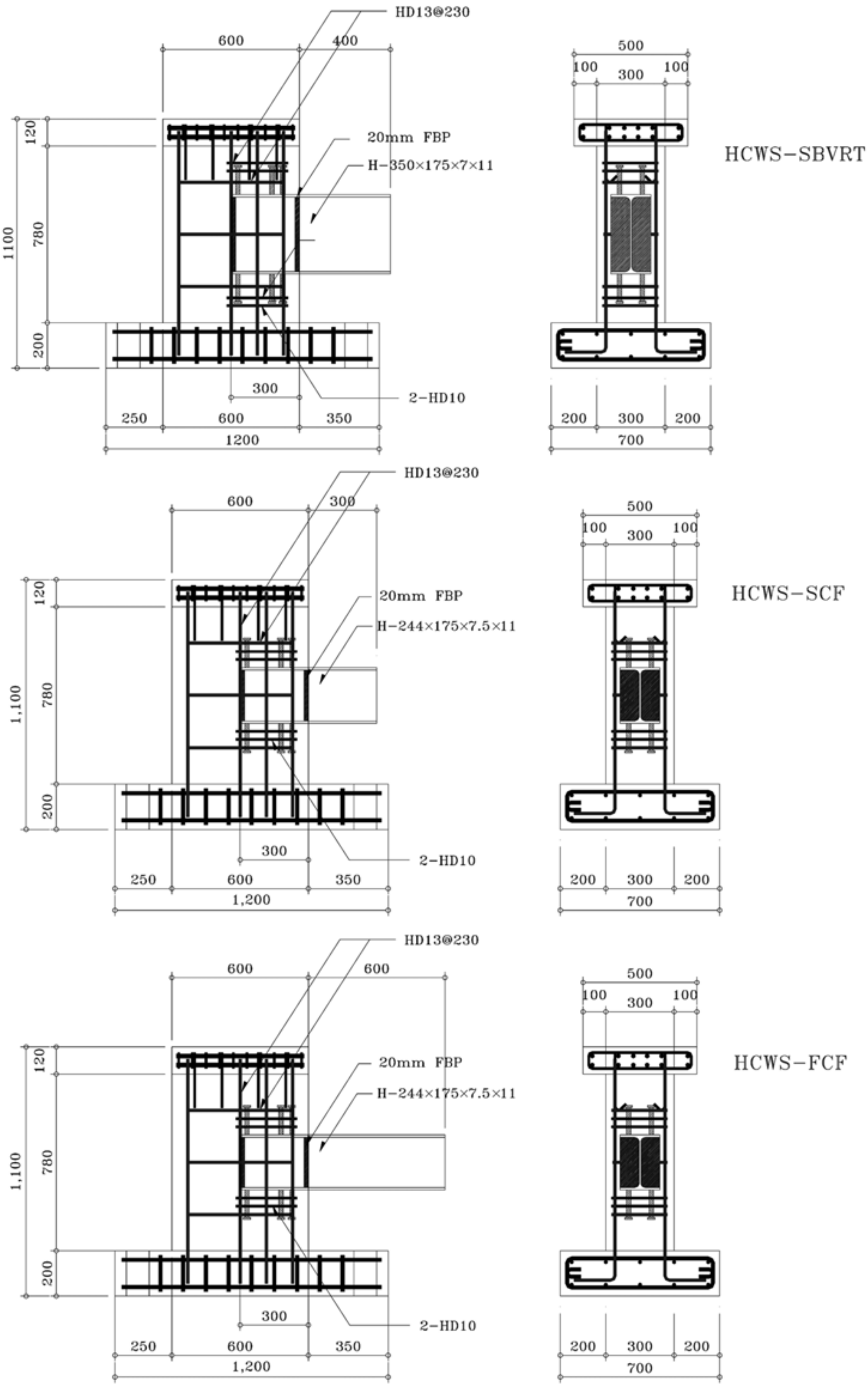

Fig. 4 Details of steel coupling beams (unit; mm)

Table 1 Test variables

Specimen name	h (mm)	b (mm)	t_w (mm)	t_f (mm)	a (mm)	l (mm)	l_e (mm)	l/H -	Loading history	Predicted failure mode
SBVRF	350	175	7	11	400	800	300	3.43	C	CF
SCF	244	175	7	11	300	600	300	3.43	C	SCF
FCF	244	175	7	11	600	1,200	300	3.43	C	FCF

*CF: Connection failure
FCF: Flexural critical failure
SCF: Shear critical failure

Table 2 Details of test specimens

Specimens \ Item	Stud bolts	Horizontal ties	Wall reinforcements		Eccentricity of vertical load e (mm)	Remark
			In wall	In connections		
SBVRT	12-ϕ19	4-HD10	HD13@230	HD13@230	+150	Connection failure $l/(M_n/V_n)$=1.8
SCF	12-ϕ19	4-HD10	HD13@230	HD13@230	+150	Shear critical $l/(M_n/V_n)$=1.4
FCF	12-ϕ19	4-HD10	HD13@230	HD19@100	+150	Flexure critical $l/(M_n/V_n)$=2.8

Table 3 Average concrete compressive strengths

Compressive strength (MPa)	Ultimate strain (μ)	Slump (mm)	Elastic modulus (GPa)	Poisson's ratio
30.0	2,340	150	26.2	0.16

*At the time of testing

Table 4 Mechanical properties of steel

Steel type \ Item		Yield strength f_y, (MPa)	Yield strain ε_y, ($\times 10^{-6}$)	Elastic modulus E_s, (GPa)	Ultimate strength f_{su}, (MPa)
Reinforcement	10 mm diameter deformed bar	398	2,325	171.2	566
	13 mm diameter deformed bar	400	2,533	157.9	555
	19 mm diameter stud bolt	362	1,701	215.8	449
Steel	Steel beam web	339	1,682	201.2	461
	Steel beam flange	352	1,827	192.7	489
Stud bolts	Face bearing plate/Stiffener	240	1,219	197	387

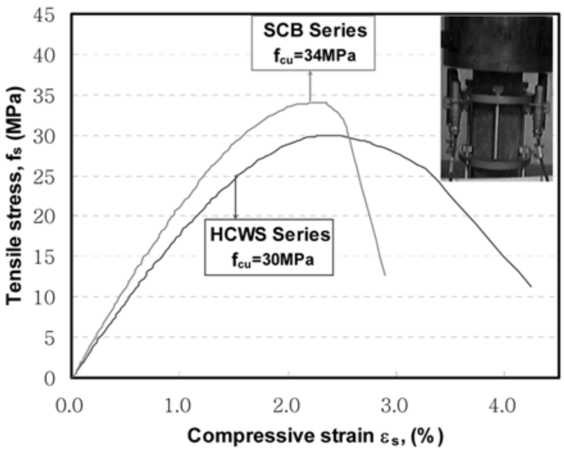

(a) Concrete

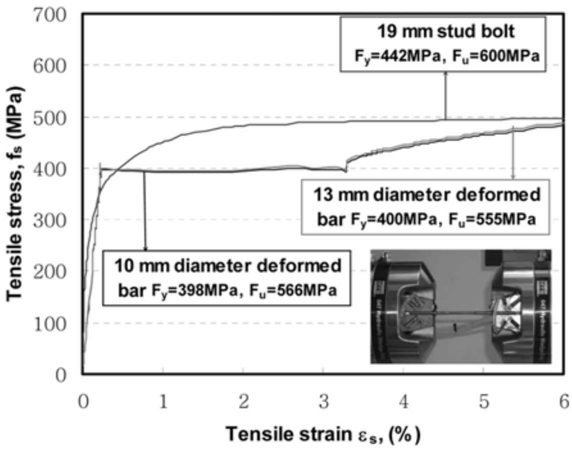

(b) Reinforcing steel

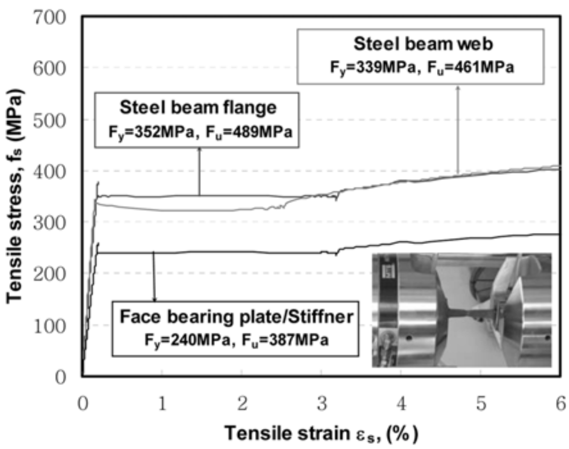

(c) Steel coupling beam flange, web, and FBP/Stiffner

Fig. 5 Material properties of concrete and steel

3.3 Experimental setup

A schematic diagram of the test apparatus is shown in Fig. 6. The test specimens were loaded with two servo-controlled actuators, a 1,000 kN hydraulic jack to apply load to the wall, and a 2,000 kN hydraulic jack to load the steel coupling beam. Both these actuators were controlled by a computer-based controller. The displacement of all the specimens was controlled to follow similar displacement histories with progressively increasing amplitude. The observed displacement history during the tests is shown in Fig. 7; θ_y indicates the rotational angle corresponding to the yielding displacement of the coupling beams. The data were acquired from the load on the hydraulic jacks, the deflection and rotational angle of the steel coupling beams, the strain of concrete in the embedment region, and the strain on the flanges and web of the steel coupling beams.

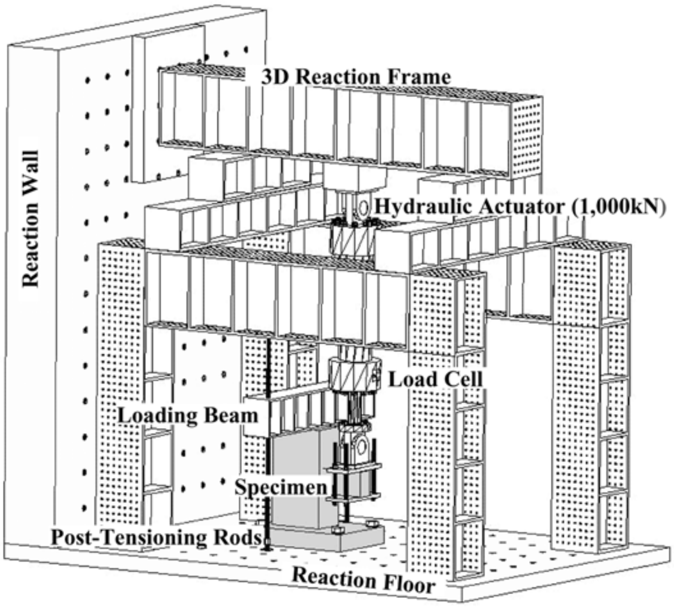

Fig. 6 Test setup

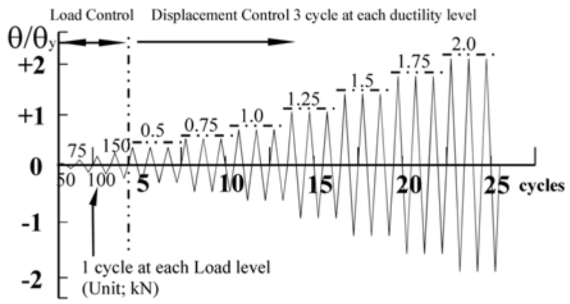

(a) Specimen SBVRT

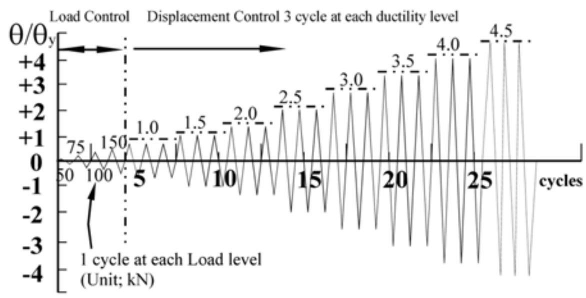

(b) Specimen SCF

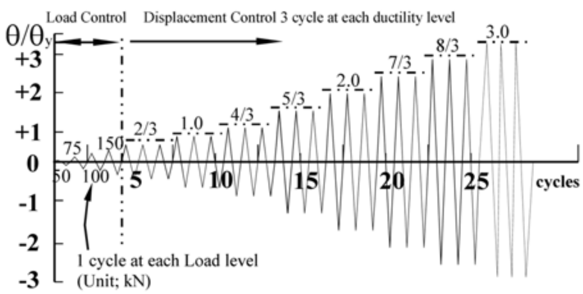

(c) Specimen FCF

Fig. 7 Displacement history

4. Experimental results

4.1 Damage and crack pattern

Fig. 8 shows the failure modes for specimens HCWS-SBVRT, HCWS-SCF, and HCWS-FCF. In specimen HCWS-SBVRT, initial vertical cracking at the steel coupling beam flange-concrete interface below embedded bottom flange was observed at a rotational angle of about 0.017 radian. Inclined cracks located at the flange-concrete interface extended from the flange across the inner face of the wall to the side faces of the wall at a rotational angle of about 0.019 radian, as shown in Fig. 8(a). Localized spalling and crushing of the concrete along the top and bottom flanges of the coupling beam at the front of the compression zone was initially observed at a rotational angle of 0.043 radian. In specimen HCWS-SCF, severe web buckling in the clear span of the steel coupling beam led to its final rupture, as shown in Fig. 8(b). Specimen HCWS-FCF, having a clear span of 1200 mm, was designed and detailed as a flexure-critical coupling beam. The response of specimen HCWS-FCF was notably less stiff than specimen HCWS-SCF. In addition, the steel beam remained elastic in shear throughout the test. Unlike shear yielding, which occurs uniformly over the entire length of a coupling beam, flexural hinge propagates away from the region of critical moment, as

(a) Specimen SBVRT

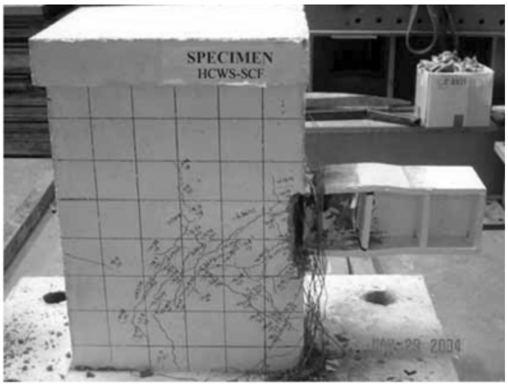

(b) Specimen SCF

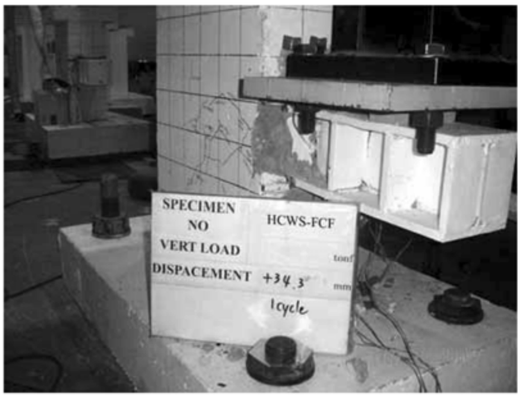

(c) Specimen FCF

Fig. 8 Cracking pattern

shown in Fig. 8(c). Observed to the failure modes, shear critical failure were most reasonable for rehabilitation or retrofitting when the buildings were damaged.

4.2 Hysteresis response

The hysteretic responses of specimens HCWS-SBVRT, HCWS-SCF, and HCWS-FCF are presented in Fig. 9. Specimen HCWS-SBVRT did not exhibit any stable spindle-type hysteretic loops caused by premature embedment region failure before the web and flange of the steel coupling beam yielded. As shown in Fig. 9(a), the hysteretic behavior of specimen HCWS-SBVRT shows a more pronounced level of pinching, which is attributed to bearing failure in the beam–wall connection region. In addition, specimen HCWS-SBVRT showed a sudden decrease in strength during the first and second cycles at the rotational angle of 0.043 radian. However, specimen

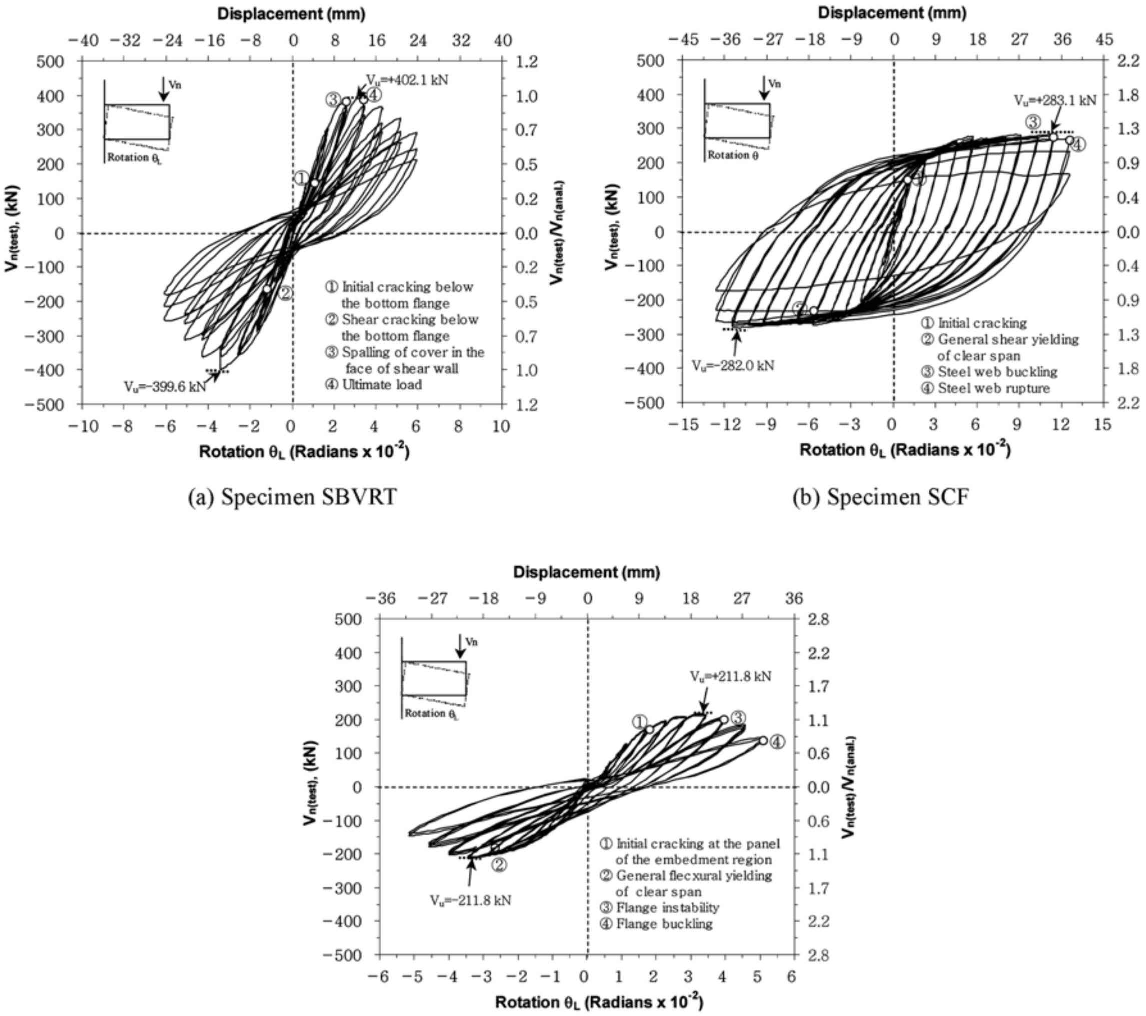

(a) Specimen SBVRT (b) Specimen SCF

(c) Specimen FCF

Fig. 9 Load-rotational angle hysteretic loops

Table 5 Test results

Specimen name	Test variables	Ultimate load (kN)		Observed failure mode	Comparison Ratio $V_{(test)}/V_{(anal.)}$
		Maximum values, $V_{(test)}$	Predicted Values, $V_{(anal.)}$		
Specimen SBVRT	Connection failure $L_b/(M_n/V_n)$=1.8	402.1	375.7	Connection failure	1.11
Specimen SCF	Shear critical $L_b/(M_n/V_n)$=1.4	283.1	222.9	Shear critical failure	1.27
Specimen FCF	Flexure critical $L_b/(M_n/V_n)$=2.8	211.8	199.8	Panel shear failure	1.06

HCWS-SCF exhibited very large, stable loops throughout the test with little strength or stiffness decay evident, as shown in Fig. 9(b). Compared with specimen HCWS-SCF, specimen HCWS-FCF exhibited a more unstable and pinched response, as shown in Fig. 9(c). This is attributed to local concrete bearing failure by buckling of the compression flange, near the shear wall face.

The relationship between normalized measured load and rotational angle is listed in Table 5. Specimens HCWS-SBVRT, HCWS-SCF, and HCWS-FCF could develop a maximum capacity equal to 402.1, 283.1, and 211.8 kN, respectively, at ultimate in the compression cycles (beam pushed down). This table showed values of $V_{n\,(test)}/V_{n\,(anal.)}$ for specimens HCWS-SBVRT, HCWS-SCF, and HCWS-FCF of 1.11, 1.27, and 1.06, respectively. The reserved strength of specimen HCWS-SCF is 14% and 20% larger than that of HCWS-SBVRT and HCWS-FCF, respectively. This can be attributed to the full shear yielding occurring in the clear span of the steel coupling beam without significant distress in the embedded region. In particular, specimen HCWS-FCF did not develop a substantially larger strength than theoretical value because of premature lateral buckling.

4.3 Energy dissipation

The energy dissipation characteristics of members are an important measure of their seismic performance. The hysteretic response of steel coupling beams is because of the combination of the yielding of the steel coupling beam outside of the coupled shear wall and the plasticity of the connection region, i.e., the yielding of the beam in the embedded region and the fracture of the surrounding concrete. Effective design would require the latter to be small. As the response of the walls remained approximately in the elastic range, the contribution of the wall segment to the total dissipated energy was insignificant. The energy dissipated by each component is, then, the area enclosed by the applied load versus the corresponding displacement. The energy dissipated by the connection and beam mechanisms is $E_{connection} = E_t + E_r$, and $E_{beam} = E_s + E_r$, respectively, where:

$$E_t = \int \delta_t dP \tag{4}$$

In the above equation, the subscript i can be either t, r, s, or f.

A graph of the cumulative dissipated energy is plotted in Fig. 10(a). As shown in Fig. 10, the total input energy for specimens HCWS-SBVRT, HCWS-SCF, and HCWS-FCF was predominately dissipated by inelastic actions in the connection region. Up to a rotation angle of about 0.0043

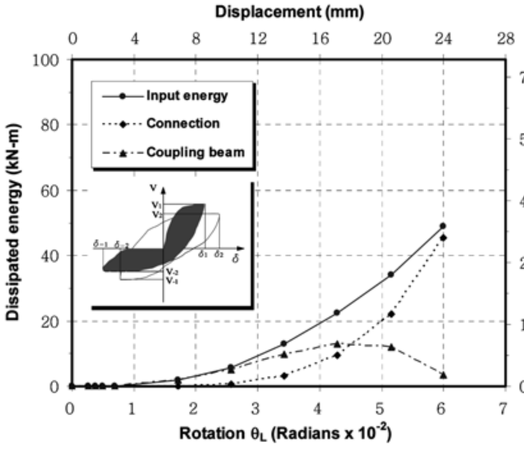

(a) Specimen SBVRT

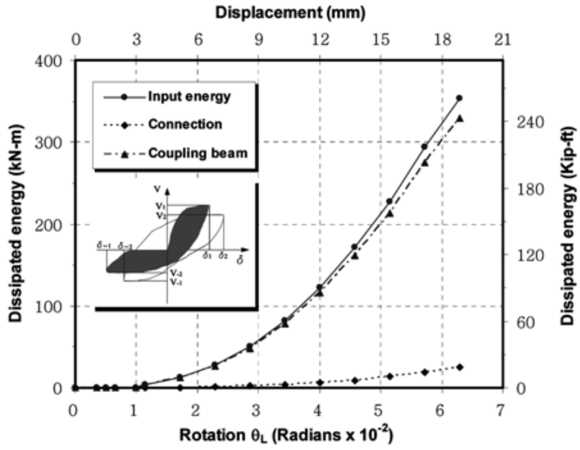

(b) Specimen SCF

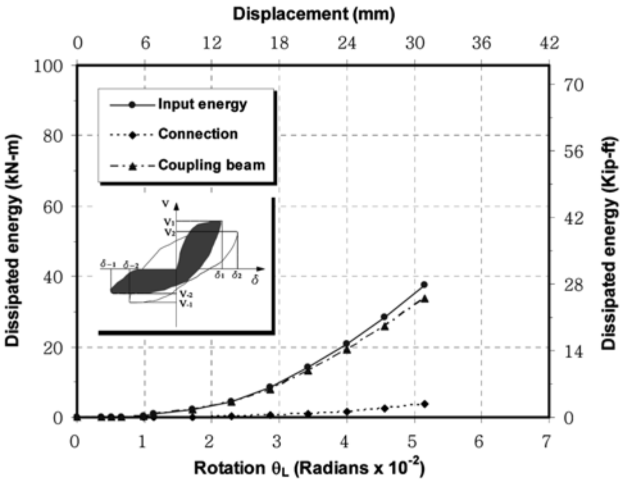

(c) Specimen FCF

Fig. 10 Distribution of dissipated energy

radian, most of the input energy for specimen HCWS-SBVRT was predominately dissipated by steel coupling beam, as shown in Fig. 10(a). However, the energy dissipated by the steel coupling beam-wall connections exceeded that dissipated by the steel coupling beam after reaching a rotational angle of about 0.0515 radian, as shown in Fig. 10(b). Beyond the rotational angle of about 0.0515 radian, excessive damage in the steel coupling beam-wall connections reversed this trend. The participation of the connection was gradually increased at higher loads and rotational angle, which produced more inelastic behavior in the steel coupling beam-wall connections. For specimen HCWS-SBVRT, the energy dissipated by the steel coupling beam-wall connections is 45.29 kN-m throughout the test and most of the total input energy was predominately dissipated by the connection. For specimen HCWS-SCF, the energy dissipated by the steel coupling beam was significantly more than that of the connection and exceeded that dissipated by the steel coupling beam-wall connection during the test, as shown in Fig. 10(b). For specimens HCWS-SCF, the

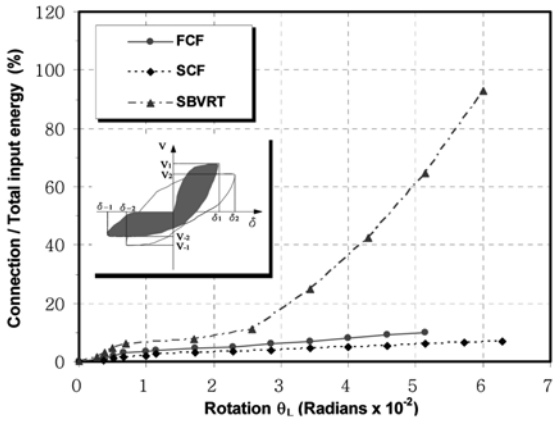

(a) Component of connection

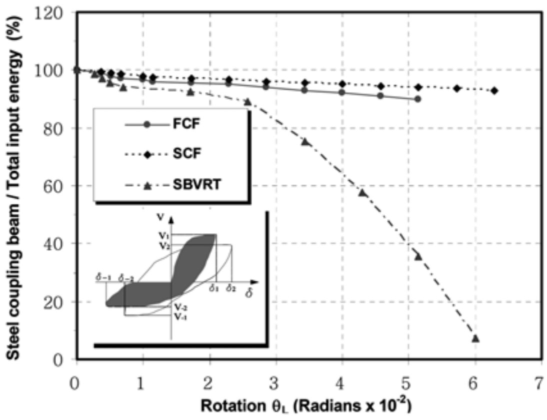

(b) Component of steel coupling beam

Fig. 11 Percentage contribution of dissipated energy

energy dissipated by the steel coupling beam at a rotation angle of about 0.0629 radian is 328.97 kN-m and about 13 times that by the steel coupling beam-wall connections. The presence of face bearing plates, stud bolts, and horizontal in the connection region evidently enhanced the energy dissipation characteristics by reducing the contribution of connection. For specimen FCF, the energy dissipation characteristics are similar to those of specimen HCWS-SCF. The energy dissipated by the steel coupling beam at a rotation angle of about 0.0515 radian is 33.67 kN-m, as shown in Fig. 10(c), and significantly lower than that of specimen HCWS-SCF.

The percentage contribution of dissipated energy versus rotation angle is plotted in Fig. 11. As shown in Fig. 11(a), the component of total input energy dissipation by steel coupling beam-wall connections for specimen HCWS-SBVRT throughout the tests was larger than in specimens HCWS-SCF and HCWS-FCF. This can be attributed to the premature connection damage of specimen HCWS-SBVRT. For specimens HCWS-SBVRT, HCWS-SCF, and HCWS-FCF, at a rotation angle of about 0.0515 radian, 65%, 6%, and 10% of the total input energy was dissipated in the steel coupling beam-wall connection region, as shown in Fig. 11(a), respectively. As shown in Fig. 11(b), the component of total input energy dissipation by steel coupling beam for specimens HCWS-SCF and HCWS-FCF throughout the tests was larger than that in specimen HCWS-SBVRT. This is attributed to the effective confinement of concrete by horizontal ties in the panel region.

Based on the observation of the three test results, shear yielding steel coupling beam (specimen HCWS-SCF) exhibit excellent ductility and energy absorption characteristics, exceeding those of connection failure member (specimen HCWS-SBVRT) or flexure yielding steel coupling beam (specimen HCWS-FCF).

4.4 Stresses and strain

4.4.1 Stresses of steel beam flange

Fig. 12 shows the distribution of stresses in the beam flanges for specimens HCWS-SBVRT, HCWS-SCF, and HCWS-FCF at three different locations. The strain gauges were attached to the beam flanges at different locations, 50 mm and 150 mm inside, and 50 mm outside the connection,

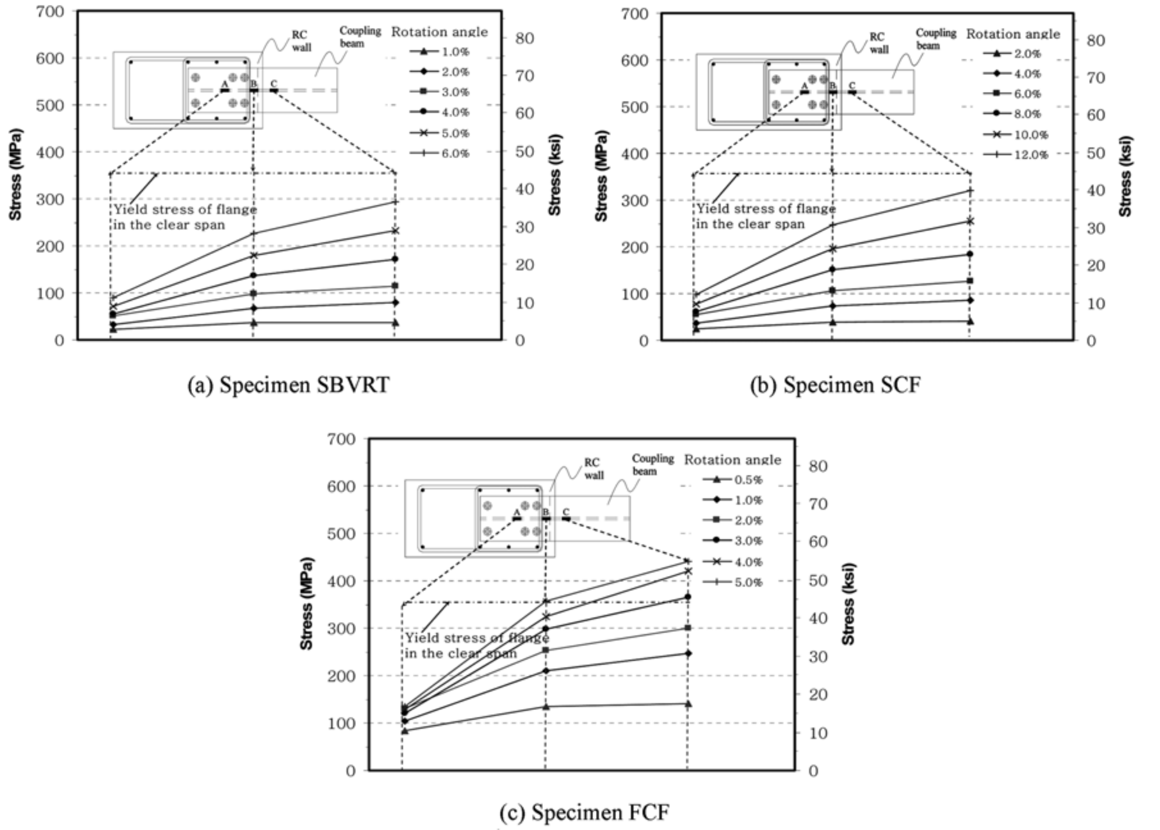

Fig. 12 Stresses of steel beam flange

to investigate the transfer of forces from the beam flanges to the connection region. As can be seen in Fig. 12, for all specimens HCWS-SBVRT, HCWS-SCF and HCWS-FCF, a slightly higher amount of the force in the steel coupling beam flanges was transferred over the location 50 mm outside the connection (point C), as indicated by the decrease in the measured strains from the steel coupling beam flange just outside the connection to that just inside the connection (point A or B). As can be seen in Figs. 12(a) and (b), for specimens HCWS-SBVRT and HCWS-SCF, a similar distribution of stresses was observed, in comparison with specimen HCWS-FCF. This is attributed to the localized spalling and crushing of the concrete in the embedment region or premature web yielding in the clear span before flange yielding of steel coupling beam occurred. As shown in Fig. 12(c), for specimen HCWS-FCF, flexural yielding of the clear span occurred at the location 50 mm outside the connection (point C) after load corresponding to the rotational angle of 0.027 radian reached.

4.4.2 Strains of horizontal ties above and below the embedded steel beam

Fig. 13 shows the distribution of strains in the horizontal ties inside the connection for specimens HCWS-SBVRT, HCWS-SCF, and HCWS-FCF. The horizontal ties located above and below the embedded steel section served two purposes. First, they provided confinement to the regions of the wall adjacent to the steel coupling beam flanges, and thus contributed to increase a bearing force in

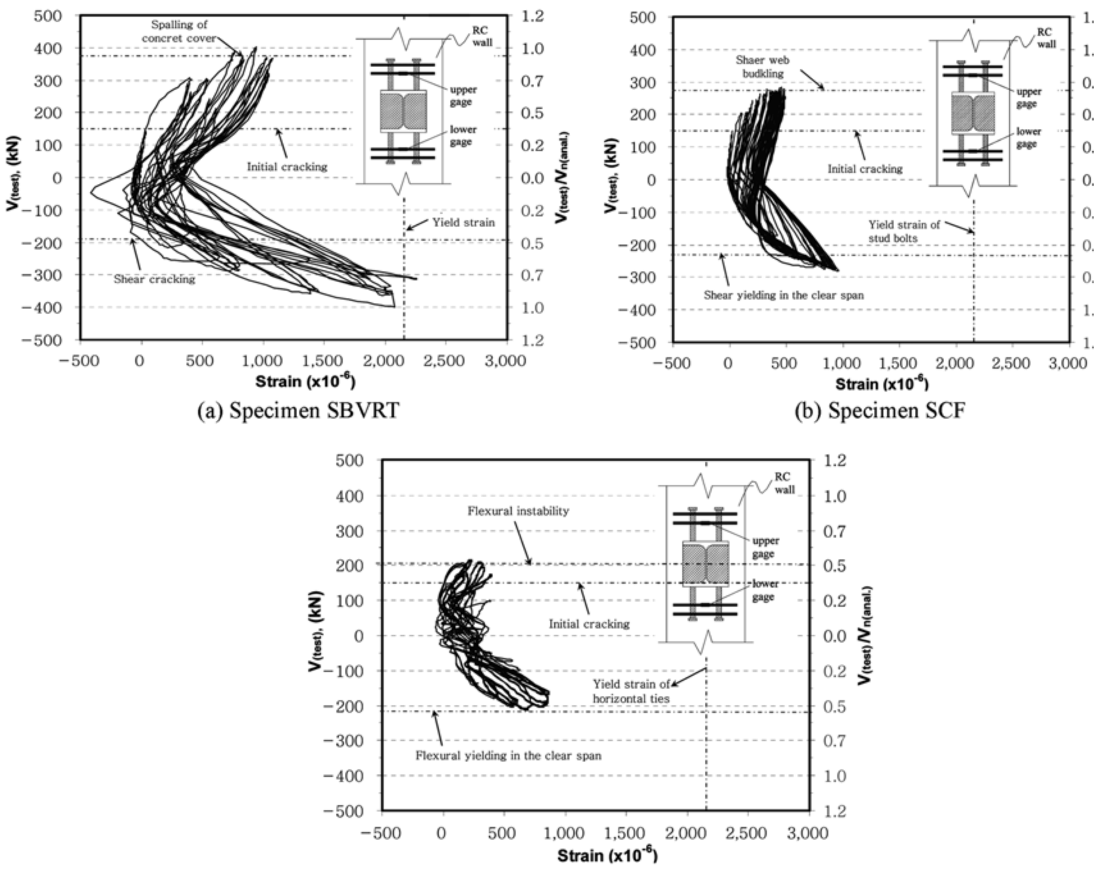

(a) Specimen SBVRT

(b) Specimen SCF

(c) Specimen FCF

Fig. 13 Strain of horizontal ties

these regions. Second, the horizontal ties adjacent to the steel coupling beam, together with reinforced concrete shear wall, played a key role in the transfer of forces from the steel coupling beam to the connection regions outside the width of the steel beam flanges. The monitoring of the strains in these stirrups helped to better understand this process of load transfer. In addition, it provided important information with regard o the distribution of tensile stress in the hoops for different locations above and below the embedded steel section. In Fig. 13(a), the different tensile strains can be observed for the positive and negative loading directions after several cracks formed in the connection. The difference in tensile strains for both directions of loading primarily depended on the cracking pattern and the location of the cracks with respect to the strain gauges. Higher tensile strains were measured in the horizontal ties placed the closest to the embedded steel beam flanges, as shown in Fig. 13(a). In Figs. 13(b) and (c), the similar tensile strains can be observed for the positive and negative loading directions up to rotational angle corresponding to the yielding of steel coupling beam. This was attributed to the premature yielding in the clear span of steel coupling beam before the failure of steel coupling beam-wall connection occurred. However, the different tensile strains can be observed for the positive and negative loading directions after yielding in the clear span of steel coupling beam occurred.

5. Conclusions

The following conclusions were derived from the results of the analysis and experiments in this study on the steel coupling beams in a hybrid wall system:

1. Existing models for calculating the embedment lengths do not consider the contribution of connection details. Therefore, model proposed in this study can be reliably used to compute the required embedment length of steel coupling beams for considering connection details of auxiliary bars and horizontal ties in a hybrid coupled shear wall.
2. In specimen HCWS-SBVRT, localized spalling and crushing of the concrete along the top and bottom flanges of the embedded steel coupling beam, was observed at the final level. In specimen HCWS-SCF, severe web buckling in the clear span of the steel coupling beam led to its final rupture. In specimen HCWS-FCF, flexural hinge in the clear span propagates away from the region of critical moment. Observed to the failure modes, shear yielding member, specimen HCWS-SCF was most reasonable for rehabilitation or retrofitting when the buildings were damaged.
3. The reserved strength of specimen HCWS-SCF is 17% and 20% larger than that of HCWS-SBVRT and HCWS-FCF, respectively. This can be attributed to the full shear yielding occurring in the clear span of the steel coupling beam without significant distress in the embedded region.
4. Shear yielding steel coupling beam (specimen HCWS-SCF) exhibit excellent ductility and energy absorption characteristics, exceeding those of connection failure member (specimen HCWS-SBVRT) or flexure yielding steel coupling beam (specimen HCWS-FCF).
5. For all specimens HCWS-SBVRT, HCWS-SCF and HCWS-FCF, a slightly higher amount of the force in the steel coupling beam flanges was transferred over the location 50 mm outside the connection (point C), as indicated by the decrease in the measured strains from the steel coupling beam flange just outside the connection to that just inside the connection (point A or B).
6. The decision to use either a shear yielding or flexure yielding steel coupling beam will depend on the span-to-depth ratio. Based on the observation of the test results from this study and a previous study, in general, shear yielding steel coupling beam will be more practical for span-to-depth ratios less than about 2.

References

ACI Committee 318. (2005), Building Code Requirements for Reinforced Concrete (ACI 318-05) and Commentary (ACI 318R-05), Farmington Hills, M.I., American Concrete Institute.

AISC. (2002), Seismic Provisions for Structural Steel Buildings. American Institute of Steel Construction.

El-Tawil, S. and Kuenzli, C. (2002), "Pushover of hybrid coupled walls. II: Analysis and behaviour", *J. Struct. Div.,* ASCE, **128**(10), 1282-1289.

Gong, B., Harries, K.A. and Shahrooz, B.M. (2000), "Behaviour and design of reinforced concrete, steel, and steel-concrete coupling beams", *Earthquake Spectra*, **16**(4), 775-799.

Harries, K.A. (1995), "Seismic design and retrofit of coupled walls using structural steel", PhD these, McGill University, Montreal, 229 pp.

Harries, K.A. (2001), "Ductility and deformability of coupling beams in reinforced concrete shear walls", *Earthquake Spectra*, **17**(3), 457-478.

IBC 2000. (2000), International Building Code, International Code Council, Falls Church, INC.
Mattock, A.H. and Gaafar, G.H. (1982), "Strength of embedded steel sections as brackets", *ACI J.,* **79**(9), 83-93.
Park, W.S. and Yun, H.D. (2005), "Seismic behaviour of steel coupling beam linking concrete shear walls", *Eng. Struct.*, JEST, **27**(7), 1024-1039.
Park, W.S., Yun, H.D., Hwang. S.K., Han, B.C. and Yang, I.L. (2005), "Shear strength of connection between steel coupling and reinforced concrete shear wall in a hybrid wall system", *J. Constructional Steel Research*, JCSR, **61**(7), 912-941.
Shahrooz, B.M., Remmetter, M.A. and Quin, F. (1993), "Seismic design and performance of composite coupled walls", *J. Struct. Div.,* ASCE, **19**(11), 3291-3309.
Shahrooz, B.M., Tunc, G. and Deason, J.T. (2002), "RC/Composite wall-steel frame hybrid building: connections and system behaviour", Report No. UC-CII 02/01, Cincinnati Infrastructure Institute.
Shahrooz, B.M., Deason, J.T. and Tunc, G. (2004a), "Outrigger beam-wall connections: Part I-component testing and development of design model", *J. Struct. Div.*, ASCE, **130**(2), 253-261.
Shahrooz, B.M., Tunc, G. and Deason, J.T. (2004b), "Outrigger beam-wall connections: Part II-subassembly testing and further modelling enhancements", *J. Struct. Div.,* ASCE, **130**(2), 262-270.
Yun, H.D., Park, W.S., Han, B.C. and Hwang, S.K. (2004), "Shear strength of steel coupling beam connections embedded in reinforced concrete shear walls", *J. of the Architectural Institute of Korea*, **20**(5), 43-50.

Notation

a : distance from beam shear to face of wall (in mm)
b_f : beam flange width (in mm)
B : width of steel coupling beams (in mm)
c : length of compression zone below embedded steel section (in mm)
C_b : resultant concrete compressive force acting on top and at back of embedded steel section, (N)
C_f : resultant concrete compressive force acting below and at front of embedded steel section, (N)
e : distance from face of wall to effective fixed point of beam (in mm)
f_b : bearing strength of concrete (in MPa)
f'_c : concrete compressive strength (in MPa)
f_h : specified yield strength of wall horizontal reinforcement (in MPa)
f_v : specified yield strength of wall vertical reinforcement (in MPa)
f_{yw} : specified yield strength of steel coupling beams web (in MPa)
f_{yf} : specified yield strength of steel coupling beams flange (in MPa)
F_y : specified yield strength of steel coupling beams (in MPa)
h : overall depth of steel coupling beams (in mm)
l : distance from ram on beam to face of wall (in mm)
l_e : embedment length (in mm)
L : effective clear span of steel coupling beams (in mm)
M_n : nominal strength of steel coupling beam (in N-mm)
t_f : beam flange thickness (in mm)
t_w : beam web thickness (in mm)
t : thickness of wall (in mm)
V_f : shear corresponding to the moment capacities (in N)
V_p : plastic shear capacities of steel coupling beam (in N)
V_r : connection strength (in N)
V_u : ultimate beam shear force (in N)
ϕ_s : strength reduction factor for steel (=0.9)